Chapter

# Optimal Integration of Series and Shunt FACTS with Wind Energy for Active Power Loss Reduction

*I. Made Wartana and Ni Putu Agustini*

## Abstract

The integration of wind energy (WE) with flexible AC transmission system (FACTS) devices into the grid to improve grid performance is one of the latest advances in renewable energy (RE) technology. This work proposes the optimal placement and size of a WE, a doubly-fed induction generator (DFIG) with two of FACTS controller, viz. thyristor-controlled series compensator (TCSC) static var compensator (SVC). The goal is to maximize system bus load (Max. LBS) and minimize active power loss (Min. $P_{loss}$) by satisfying various safety and stability constraints. Newton Raphson's power flow study involving TCSC, SVC, and DFIG is a bi-objective that meets multiple constraints: lines, generation, voltage limits, and small signal stability. A variant of the genetic algorithm, non-dominated sorting GA II (NSGA-II), was applied to solve the contradictory bi-objective optimization problem. A modified standard and practical test system, the IEEE 14-bus and the Indonesia Java Bali 24-bus, integrated with DFIG, TCSC, and SVC, were simulated to investigate the efficacy of the suggested technique. The simulation shows that the optimal placement and size of DFIG with both FACTS can improve system performance with all system loading conditions and meet all system constraints.

**Keywords:** doubly-fed induction generator, load bus system, small signal stability, wind energy, unified power flow controller

## 1. Introduction

In the last decade, recent advances in renewable energy (RE) technology have discussed the development of the technology industry, which includes conversion, storage, production, and management, especially wind energy systems, solar, hydropower, geothermal energy, bioenergy, and hydrogen production [1, 2]. The development of this large-scale energy technology and its impact on the global economy and electricity capacity is a fascinating study, especially related to system

optimization and sizing, resource assessment and deployment, instrumentation and control, modeling and simulation, regulation, and policy [3–5].

The development of renewable energy sources (RES) resources into the mainstream electricity sector has increased in recent years as awareness of environmental issues and efforts to reduce dependence on fossil fuel resources increase. Wind energy (WE) is assumed to have the most commercial technics and economic prospects among the various renewable resources. Integrating the RES represented as a Distributed Generation (DG) into the grid has received wide attention and scope in power systems [6, 7]. In addition, DG can help utilize distributed energy sources with relatively small resources and reduce the use of electrical power transmission capacity [8]. Most DGs are located near the load center, and some types of DGs also provide reactive power to support the power system [9].

On the other hand, since DGs are installed close to the load, they can minimize active power loss (Min. $P_{loss}$) and increase profile voltage, improving system performance [10]. Another advantage of integrating DGs into the grid is that they can delay investments in transmission lines and the construction of large power plants. Above all, the second option/advantage has been utilized in this chapter to maximize the load bus system (Max.-LBS) by optimal placement of DGs into the grid [11]. However, some DGs, particularly wind generation systems, do not generate almost negligible reactive power. Numerous other mechanisms have been used to compensate the system when the DG can no longer support the system's reactive power requirements.

The integration of various DG technologies and flexible alternating current transmission systems (FACTS) into the grid started one of the significant management concerns for professional engineers [12, 13]. Various studies have extensively studied grids involving RES and FACTS devices to improve security, power quality, system stability, and optimal reactive power delivery using different latest optimization techniques [9, 10]. Some essential technical benefits are increasing the voltage profile with Min. $P_{loss}$ and Max.-LBS. All the while enhancing the power system's security, reliability, and stability, thereby increasing the overall energy efficiency [14], furthermore relieving transmission and distribution congestion. In addition, DG utilizes the small energy resources available near the load center, thereby increasing energy access [15, 16]. Moreover, by installing FACTS series and shunts in the system, apart from increasing the performance of the system, it can also help secure and restore network operations during emergencies and after power outages. However, integrating a wide variety of DG technology and FACTS into the grid has become one of the significant management concerns for operational people.

Numerous works have been done on the optimal allocation of DG for different purposes. Different approach techniques have been suggested, that is, Genetic Algorithm (GA) [17], PSO [18], and an efficient hybrid approach distribution networks [19] for optimal location and settings of multi-types of DG. The optimal DG placement has been compared using CSA, GSA, PSO, and the firefly algorithm for the minimum real power loss in a radial distribution system [20, 21]. However, the system stability and security constraints have not been exclusively considered by Max.-LBS within any grid condition and their impact on the transmission loss with the DG placement.

From these literary works, it can be observed that most of the problems in optimal DG locations are often disclosed separately as a matter of mono-objective optimization [22–24]. Awkwardly, formulating the problems as a mono-objective optimization

is not entirely practical. However, it is always good to utilize optimal DG placement with two conflicting objectives, considering the security and stability of the system formulated as a multi-objective problem and solved simultaneously [10].

In this work, a multi-objective problem has been formulated by Max. LBS by optimal location and settings of a DG, viz. wind generation system or farm, while maintaining the system security and stability margin within an acceptable range. Utilizing DG optimal placement, the Max. LBS and the Min. $P_{loss}$ can be done simultaneously. The multi-objective problems have been solved simultaneously using the novel variant of GA specialized in multi-objective optimization, namely the NSGA-II by optimal location and sizing of the DG.

## 2. System component modeling

### 2.1 Wind turbine generator modeling

Of the two basic types of wind turbine generators (WTG) available, the second category is variable speed. This popular type of WTG is known as a double induction generator (DFIG) and synchronous direct-drive generator [25]. This type in addition to offering increased efficiency in capturing energy from the wind over a broader range of wind speeds also has better power quality and the ability to regulate power factors, both consuming and generating reactive power. **Figure 1** shows a DFIG type of WTG, where the rotor through a back-to-back ac/dc/ac converter is connected to the grid, while the stator is connected directly to the grid [26, 27]. In this model, the generator is decoupled from the grid since the dynamics of the stator, and rotor flux is fast compared to the grid dynamics and the converter controls; consequently, the steady-state electrical equation of the DFIG is assumed as (1):
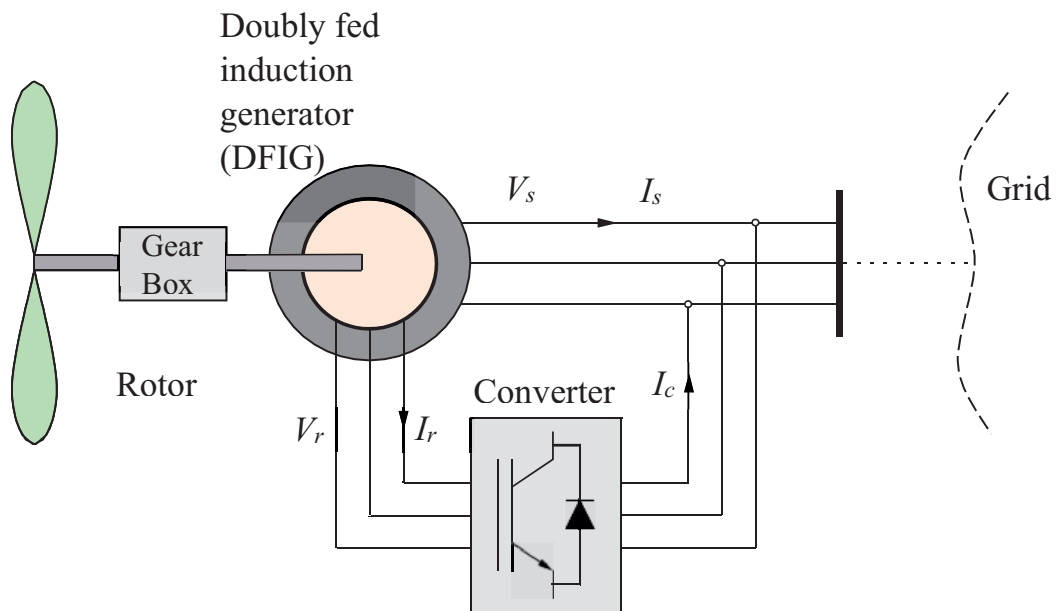


**Figure 1.**
*Variable speed of WTD with DFIG modeling.*

$$\left.\begin{aligned}
v_{ds} &= -R_s i_{ds} + \big((X_s + X_m)i_{qs} + X_m i_{qr}\big) \\
v_{qs} &= -R_s i_{qs} + \big((X_s + X_m)i_{ds} + X_m i_{dr}\big) \\
v_{dr} &= -R_R i_{dr} + (1 - \omega_m)\big((X_R + X_m)i_{qr} + X_m i_{qs}\big) \\
v_{qr} &= -R_R i_{qr} + (1 - \omega_m)\big((X_R + X_m)i_{dr} + X_m i_{ds}\big)
\end{aligned}\right\} \tag{1}$$

where $v_{ds}$ and $v_{qs}$ are d-axis and q-axis stator voltage, respectively, $v_{dx}$ and $v_{qr}$ are d- and q-axis rotor voltage, respectively, $i_{dx}$ and $vi_{qx}$ are d-axis and q-axis rotor current, respectively, $R_s$ and $R_r$ are stator and rotor resistance, respectively, $X_s$ and $X_m$ are stator and magnetization reactance, respectively, $X_r$ and $\omega_m$ are rotor reactance and the rotor speed, respectively.

Whereas both $v_{ds}$ and $v_{qs}$ are functions of the grid magnitude and phase as formulated in Eq. (2):

$$\left.\begin{aligned}
V_{ds} &= V \sin(-\theta) \\
V_{qs} &= V \cos(-\theta)
\end{aligned}\right\} \tag{2}$$

The generator's active and reactive power depends on the stator and current converter, as shown in Eq. (3):

$$\left.\begin{aligned}
P &= v\,i + v\,i + v\,i + v\,i \\
Q &= v_{qs}i_{ds} + v_{ds}i_{qs} + v_{qc}i_{dc} + v_{dc}i_{qc}
\end{aligned}\right\} \tag{3}$$

## 2.2 Thyristor controlled series compensator (TCSC) modeling

One popular type of FACTS series will be used in this study, namely the thyristor-controlled series compensator (TCSC). The function of installing these devices into the grid, not only to increase the series capacitance, but also to reduce the total reactance of the grid. Moreover, TCSC is also used for achieving maximum flexibility in managing the grid reactance [28]. Although the cost of the device was a little bit more expensive, compare similar the FACTS, they provide real-time capabilities to respond to the grid conditions. It is done by dynamically adjusting the amount of reactance compensated [29]. **Figure 2** shows TCSC modeling as a constant capacitive reactance on a transmission line connected between bus-i and j. This capacitive reactance modifies the line reactance $x_{ij}$, during power flow analysis, as stated in (4) [30].
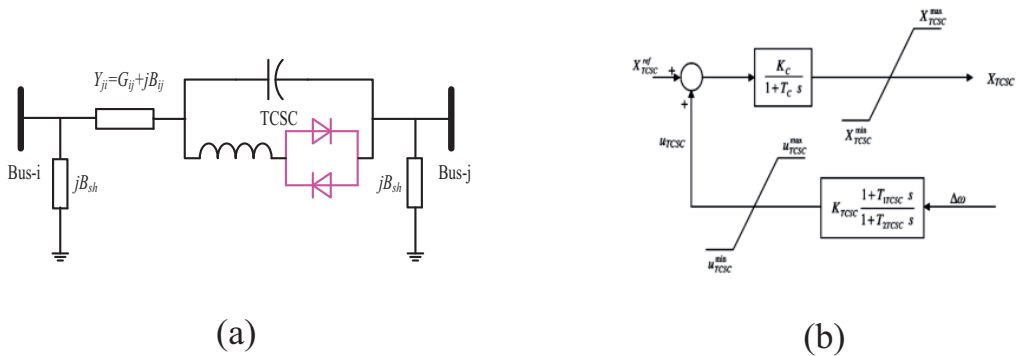


(a)                                                      (b)

**Figure 2.**
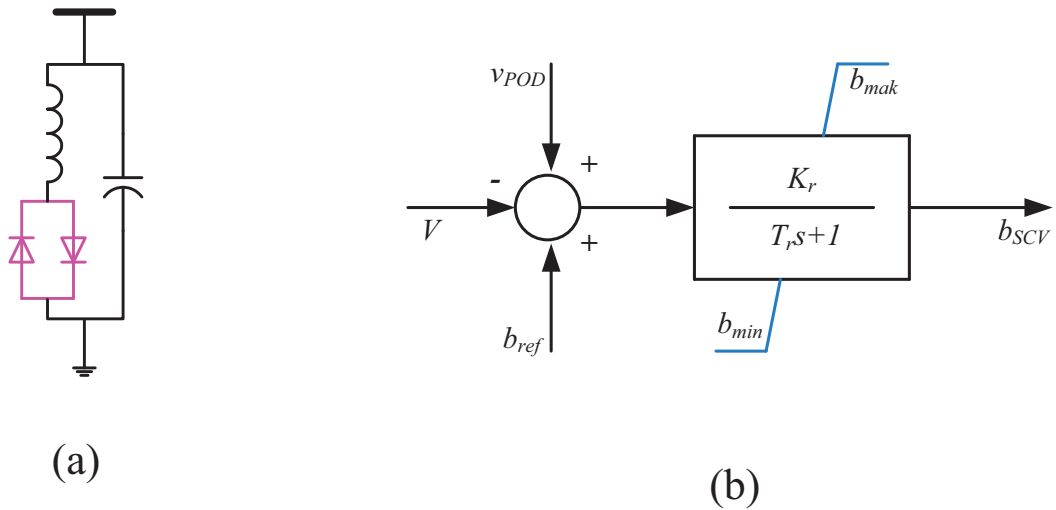*TCSC modeling. (a) TCSC model in power system; (b) block diagram model of TCSC.*

**Figure 3.**
*SVC modeling. (a) SVC model in power system; (b) block diagram model of SVC.*

$$x'_{ij} = (1 - c_p)x_{ij} \qquad (4)$$

## 2.3 Static var compensator (SVC) modeling

SVC is also a popular type of FACTS which is a shunt-connected variable reactor to the bus that can inject or absorb reactive power to regulate the bus voltage. Because it can provide instant reactive power for voltage support having two regions, capacitive and inductive, either in capacitive or inductive mode, SVC can inject reactive and inductive power [31]. **Figure 3** depicted the SVC modeling as an equivalent series of susceptance variables depending on the node requirements. The differential and algebraic equations formulated in (5) and (6) in the model give the total reactance $b_{SVC}$ and reactive power injected at the SVC node [32].

$$\dot{b}_{SVC} = (K_r(V_{ref} + v_{POD} - V) - b_{SVC})/T_r \qquad (5)$$

$$Q = b_{SVC}V^2 \qquad (6)$$

where the maximum and minimum susceptance (p.u) are presented by $b_{max}$ and $b_{min}$, respectively, and the input signal for power system oscillation damping is modeled as $v_{POD}$.

## 3. Problem formulation

Increasing the load to attain the maximum load bus system (Max. LBS) but with minimum line power loss (Min. $P_{loss}$) was preferred as two conflicting optimization objectives. To solve the optimization algorithm developed whereas maintaining the security and stability of all systems, NSGA-II can handle it simultaneously. The problem is formulated as a discrete-continuous multi-objective optimization with the real constraint $F(\mathbf{x}, \mathbf{u})$. While the dependent and control variables are represented by $\mathbf{x}$ and $\mathbf{u}$ as formulated in Eqs. (7) and (8), respectively [33].

$$\text{Minimize } F\,(\mathbf{x},\,\mathbf{u}) = [-F_1\,(\mathbf{x},\,\mathbf{u}),\, F_2\,(\mathbf{x},\,\mathbf{u})] \tag{7}$$

$$\text{Subject to}: g_i\,(\mathbf{x},\,\mathbf{u}) = 0 \ i = 1,\dots,M$$

$$h_j\,(\mathbf{x},\,\mathbf{u}) \leq 0 \ j = 1,\dots,N \tag{8}$$

where the objective functions to be optimized are presented by $F_1$ and $F_2$, respectively. The $i$th equality and the $j$th inequality constraints are gi and $h_j$, respectively. The number of equality and inequality constraints are M and $N$, respectively.

## 3.1 Max. LBS

This research is to maximize the load bus system (Max. LBS) chosen as the first objective function with a load increase scenario as formulated in (9) and (10), respectively:

$$\text{Maximize } F_1\,(\mathbf{x},\,\mathbf{u},\,\lambda) \tag{9}$$

$$\text{Subject to}: VL = \sum_{i=1}^{N_L} OLL_i + \sum_{i=1}^{N_L} BVV_i \tag{10}$$

where the system load parameter is λ, derived in (9), *VL*, which are the sum of $OLL_i$ and $BVV_j$ stated at (12) and (13), respectively. Both characterize the thermal and bus violation limit factors. The total number of transmission lines and load busses are indicated as $N_L$ and $N_E$, respectively [34].

$$\lambda = \exp \lfloor \gamma \left| \lambda_f - \lambda_f^{\max} \right| \rfloor; \lambda_f \in \left[1,\, \lambda_f^{\max}\right] \tag{11}$$

where the slope adjustment coefficient of a function is denoted as $\gamma$, the active and reactive power demand, $P_{Di}$ and $Q_{Di}$, as formulated in (12) and (13), respectively revealed in the load factor $\lambda_f$ which has a maximum value of $\lambda_f^{max}$.

$$P_{Di}(\lambda_f) = (\lambda_f)P_{Di} \tag{12}$$

$$Q_{Di}(\lambda_f) = (\lambda_f)Q_{Di} \tag{13}$$

The first term of Eq. (10), $OLL_i$, formulated at Eq. (13) represents the indices of the system security state in which its value is equal to 1 if the $j$th line loading is less than its rating. Otherwise, it increases logarithm with the overload as given in (14):

$$OLL_i = \begin{cases} 1; \text{if } P_{ij} \leq P_{ij}^{\max} \\ \exp\left(\Gamma_{OLL}\left|1 - \dfrac{P_{ij}}{P_{ij}^{\max}}\right|\right); \text{if } P_{ij} \geq P_{ij}^{\max} \end{cases} \tag{14}$$

where $P_{ij}$ and $P_{ij}^{max}$ are the real power flow between bus-i and j and its thermal limit, respectively. Whereas the coefficient used to adjust the slope of the exponential function is $\Gamma_{OLL}$. The second term, $BVV_j$, state of (10), is the indices of the system security associated with the bus voltage violation factor at bus-j as defined in (15):

$$BVV_i = \begin{cases} 1; \text{if } 0.9 \leq V_b \leq 1.1 \\ \exp\left(\Gamma_{BVV}|1 - V_b|\right); \text{otherwise} \end{cases} \tag{15}$$

where $\Gamma_{BVV}$ is the coefficient used to adjust the slope of the exponential function, similar to Eq. (13), If $BVV_j$ is equal to 1, the voltage level drops between their minimum and maximum limits; otherwise, the voltage deviation increases exponentially.

## 3.2 Min. $P_{loss}$

The second objective function is to minimize the line power loss ($P_{loss}$) of the transmission line as expressed in (16) [35].

$$F_2(\mathbf{x}, \mathbf{u}) = P_{loss} = \sum_{k=1}^{nl} g_k \left[ V_i^2 + V_j^2 - 2V_i V_j \cos\left(\delta_1 - \delta_j\right) \right] \qquad (16)$$

where $nl$ is the transmission line numbers, $g_k$ is the conductance of $k$th line; whereas $V_i \angle \delta_i$ is the voltage on the end bus-$i$ and $V_j \angle \delta_j$ is the voltage on the end bus-$j$ of the $k$th line.

## 3.3 The equality constraint

At every node, the typical load flow eqs. [36] are denoted as their equality constraints expressed in (17).

$$P_{Gi} = P_{Li} + V_i \sum_{i=1}^{Nb} V_j \left( G_{ij} \cos\delta_{ij} + G_{ij} \sin\delta_{ij} \right); \quad i = 1,2,\cdots N_b$$

$$Q_{Gi} = Q_{Li} + V_i \sum_{i=1}^{Nb} V_j \left( G_{ij} \cos\delta_{ij} + G_{ij} \sin\delta_{ij} \right); \quad i = 1,2,\cdots N_b$$

$$(17)$$

where $N_b$ is the of busses number.

## 3.4 Small-signal stability

This stability constraint represents the dynamic performance of the power system, and is related to the weakening of the electromechanical oscillation mode. The oscillation behavior is similar to (i) the variation of electrical torque developed by the synchronous machines when the rotors angle changes; and (ii) the inertia of the rotor. This oscillation mode is usually associated with a range of frequencies between 0.5 and 4 Hz [37]. A set of differential-algebraic equations (DAE), used for small signal stability analysis, is formulated as (1):

$$\left. \begin{array}{l} x = f(x,\ y) \\ 0 = g(x,\ y) \end{array} \right\} \qquad (18)$$

where the vectors of the state and algebraic variables are represented by x and y, respectively. To calculate the state matrix $A_s$ uses the complete Jacobian matrix manipulation $A_C$ by determining the linearization of the DAE system in (19):

$$\begin{bmatrix} \Delta x \\ 0 \end{bmatrix} = \begin{bmatrix} \nabla_x f & \nabla_y f \\ \nabla_x g & \nabla_y g \end{bmatrix} \begin{bmatrix} \Delta x \\ \Delta y \end{bmatrix} = [A_c] \begin{bmatrix} \Delta x \\ \Delta y \end{bmatrix} \qquad (19)$$

By simply eliminating the algebraic variables of the state matrix $A_s$ the (20) attained. Implicitly this equation assumes that the Jacobian model's power flow is non-singular:

$$A_s = F_x - F_y G_y^{-1} G_x \tag{20}$$

The matrix leads to the calculation of eigenvalues in the S-domain, which states that if the real part of the eigenvalues is less than 0, then the system is stable.

## 3.5 Fast voltage stability index

Fast Voltage Stability Index (FVSI) [38], is one of the stability indices used to guarantee safe bus loading in this study as formulated in (21):

$$FVSI_{ij} = \frac{4Z^2 Q_J}{V_I^2 X} \tag{21}$$

Since its value is close to 1.00 specifies that the line is potential the point of instability, but if the total goes above 1.00, a quick voltage drop can happen on one of the busses coupled to the line producing the system to collapse.

## 3.6 Line stability factor (LQP)

Eq. (22) formulates the line stability factor (LQP) applied to [39], to ensure the system stability index if the value is less than 1.00:

$$LQP_{ij} = 4 \left( \frac{X}{V_i^2} \right) \left( \frac{X}{V_i^2} P_I^2 + Q_j \right) \tag{22}$$

## 4. Brief description of the NSGA-II

The technique developed by K. Deb [40] is included in the Elitist multi-objective evolutionary algorithm category with a fast non-dominated sorting approach with low computational complexity. In the NSGA-II, elite preservative operators favor the elite of a population by allowing them to be taken directly to the next generation. In this process,good solutions that are found in the beginning will never disappear unless better solutions are found. The bi-objective of the multi-objective optimization algorithm is maintained by using a fitness assignment scheme that prefers a non-dominated solution. The population in this technique is initialized as usual as an evolution algorithm solves multi-objective optimization problems [41]. The NSGA-II procedure is presented in **Figure 4**.

For every generation k does:

a. With size N, create a random parent population;

b. Based on non-dominance, then sort the population;

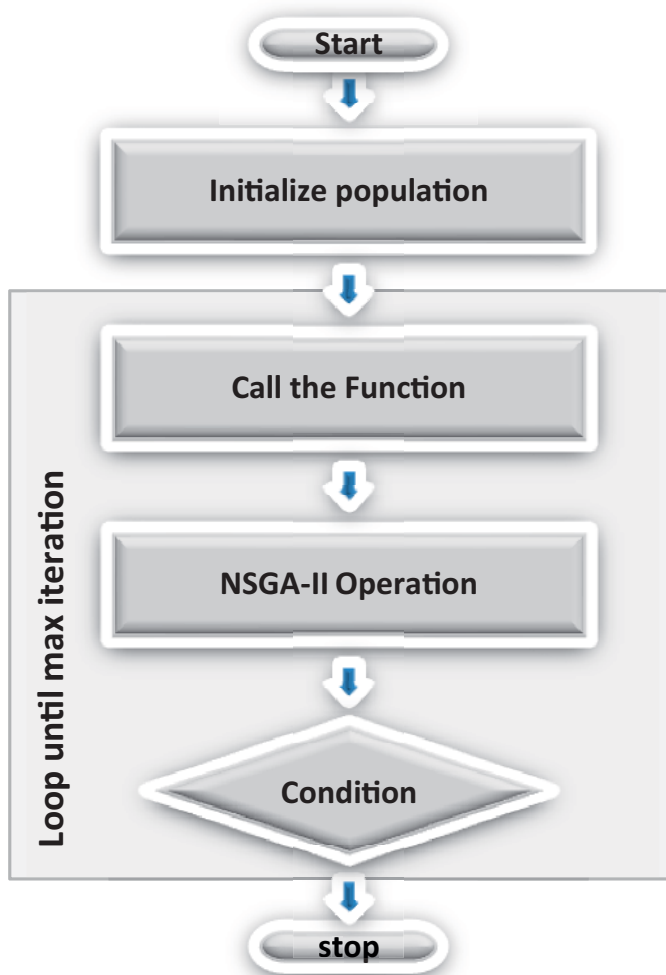c. With its non-dominant level (assumed to minimize fitness), assign each fitness solution (or rating) the same;

**Figure 4.**
*NSGA-II procedure.*

d. Create a new offspring population of size N using the usual binary tournament selection, recombination, and mutation operators for;

e. To form an expanded population of size 2 N, combine the offspring and parent populations;

f. Based on non-dominance, sort the expanded population;

g. With the individuals from the sorting sequence starting from the best, fill in the new population of size N;

h. To ensure diversity, if the front can only partially fill the next generation (This strategy is called "niching"), call the crowding comparison operator;

i. So that until the stopping criteria are met, perhaps a certain number of generations, repeat steps (2) to (8).

Determining a compromise solution suitable for all non-inferior alternatives depends on the decision-making agency's subjective preferences, the decision maker (DM), so it is not just a matter of hanging. It is reasonable to assume that DM may have imprecise or objective ambiguity for each objective function due to the ambiguous nature of DM assessment. Thus, each membership function is not only determined by intuitive knowledge but also by the experience of DM, which is introduced to represent the purpose of each objective function, as formulated in (23) [42].

$$\mu_i = \begin{cases} 1 & F_i \leq F_i^{\min} \\ \dfrac{F_i^{\max} - F_i}{F_i^{\max} - F_i^{\min}} & F_i^{\max} < F_i < F_i^{\min} \quad in \\ 0 & F_i \geq F_i^{\max} \end{cases} \qquad (23)$$

where, $F_i^{max}$ and $F_i^{min}$ are the maximum and minimum values of the $i$th objective function among all non-dominated solutions, respectively. A membership function that diverges between 0 and 1 is denoted by $\mu_i$, where $\mu = 1$ and $\mu = 0$ signify complete compatibility and mismatch, respectively, of solutions with the set [43]. Meanwhile, Eq. (24) formulates a normalized membership function k for each calculated non-dominated solution k.

$$\mu^k = \frac{\sum_{i=1}^{N_{obj}} \mu_i^k}{\sum_{k=1}^{M} \sum_{i=1}^{N_{obj}} \mu_i^k} \qquad (24)$$

where, the amounts of objective functions and non-dominated solutions are denoted as $N_{obj}$ and $M$, respectively. A membership function of non-dominated solutions in a fuzzy set can be deliberated in the function $\mu^k$, where the solution devouring the maximum membership in the fuzzy set is deliberated as the best compromise solution.

a. The NSGA-II implementation for optimal integration of WTG with FACTS.

Such as validated in this study, the bi-objectives of this study are to attain Max. LBS by optimal location and settings of one type of WTG with two series or shunt FACTS controller into the grid to minimize the $P_{loss}$ (Min. $P_{loss}$) of transmission lines while keeping the system security and stability and margins. Eqs. (7) and (8) previously formulated the optimization problems which are expressed as a bi-objective optimization problems. To investigate both conflicting objectives simultaneously, the NSGA-II techniques have been employed in numerous case studies: i) base case: without WTG and FACTS device; ii) Case-1: WTG only; iii); Case-2: TCSC only; Case-3: WTG and TCSC, Case-4: SVC only and Case-5: WTG and SVC. The point of best compromise solution (best CS) from the Pareto front is associated with the optimal solution of the equivalent objectives optimized with Max. LBS is the best LBS, and Min. $P_{loss}$ is the best $P_{loss}$ for respectively of the bi-objectives.

## 5. System studies and result discussions

The technique proposed in this study has been tested on the modification of the standard test system IEEE 14-bus [36] and the practical test system, namely the

Indonesia Java-Bali 24-bus system [22]. The loads are denoted as constant power or PQ loads with constant power factors and changed based on Eqs. (11) and (12). Furthermore, one type of wind field, DFIG, can transmit large amounts of active power to the system and consumes and produces reactive power optimally integrated into the grid. Simultaneously two types of series and shunt of FACTS devices, TCSC or SVC, are integrated into the grid to control various stability and security of the system due to increased LBS. The decision variables are the location, sizing, and settings of DFIG and the FACTS. The number of the FACTS is fixed at one, and their constraints are chosen at the beginning. All the load busses system is nominated to be the optimal location of DFIG or SVC placement. At the same time, all the grid lines are nominated to be the optimal location of the TCSC controller, which is deliberated as a discreet variable. The parameters of NSGA-II for entirely optimization cases are given in **Table 1**.

### 5.1 IEEE 14-bus system

#### 5.1.1 Base case: Without FACTS devices and WTG

In the base case condition, where the grid is not connected to FACTS devices and WTG, Pareto fronts are gained from the simulation of the NSGA-II technique, as depicted in **Figure 5**. Max. LBS and Min. $P_{loss}$ was obtained at 149.59% and 0.1704%, respectively, but the best CS achieved by $P_{loss}$ was slightly lower than the previous result of 1.1625%, as well as the LBS which slightly decreased by 111.51%. All system stability in this condition is not considered.

#### 5.1.2 Case-1: WTG only

Connecting the WTG type DFIG on the grid obtained a non-dominated solution, as shown by the Pareto front in **Figure 6**. In this case, the best LBS and $P_{loss}$ gained is 157.40% and 0.2239% by placing WTG on busses 14 and 8, respectively. The best value is similar to the previous base case; the increase in LBS is much higher even though the value of the $P_{loss}$ has also increased slightly. Based on **Figure 6**, it can also be seen that the best CS value for $P_{loss}$ is almost similar to the base case value of 0.1772%. The LBS value is slightly lower at 112.24% with optimal WTG location on bus 8 with both active and reactive power of 49.91 MW and −11.46 MVar, respectively. **Figure 7** proves that in this condition, the system is stable in terms of small-signal stability, which is expressed by negative values of all pairs of eigenvalues in the S-plane.

#### 5.1.3 Case-2: TCSC only

Optimal placement of TCSC, as one type of FACTS series, on the grid for Case-2 has been carried out and produces a Pareto front as given in **Figure 8**. From the figure,

| Population | Generations | Pool size | Tour size | $\eta_c$ |
|---|---|---|---|---|
| 100 | 50 | 25 | 2 | 20 |

**Table 1.**
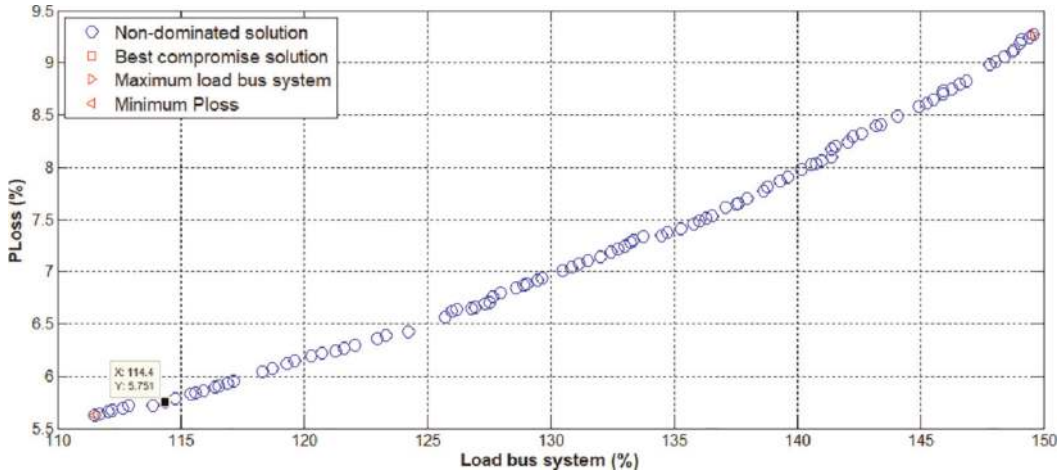*NSGA-II parameters.*

**Figure 5.**
*Pareto front of the base case.*
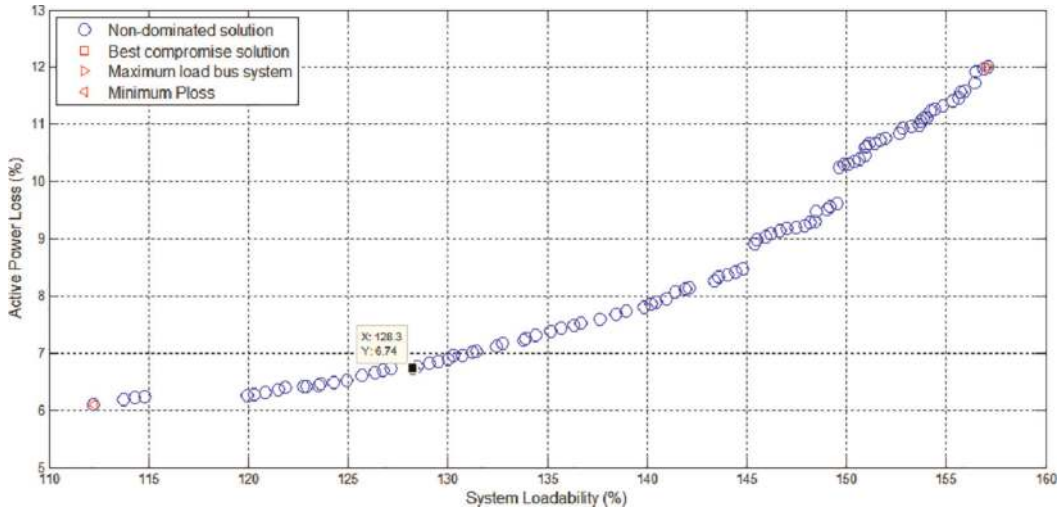
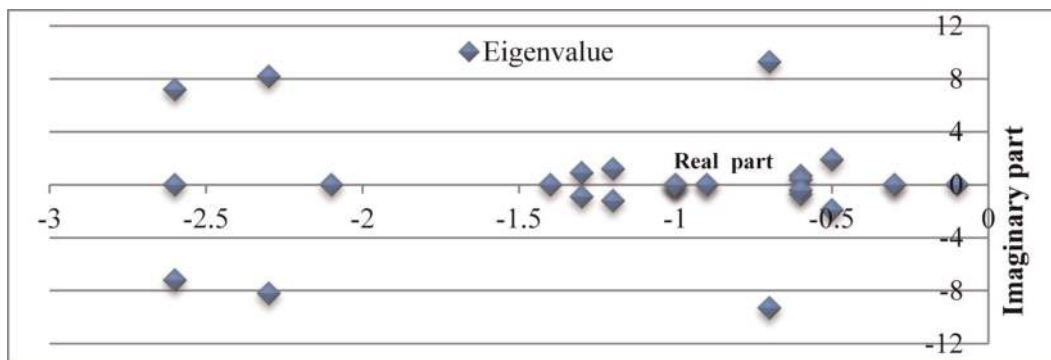

**Figure 6.**
*Pareto front of Case-1.*



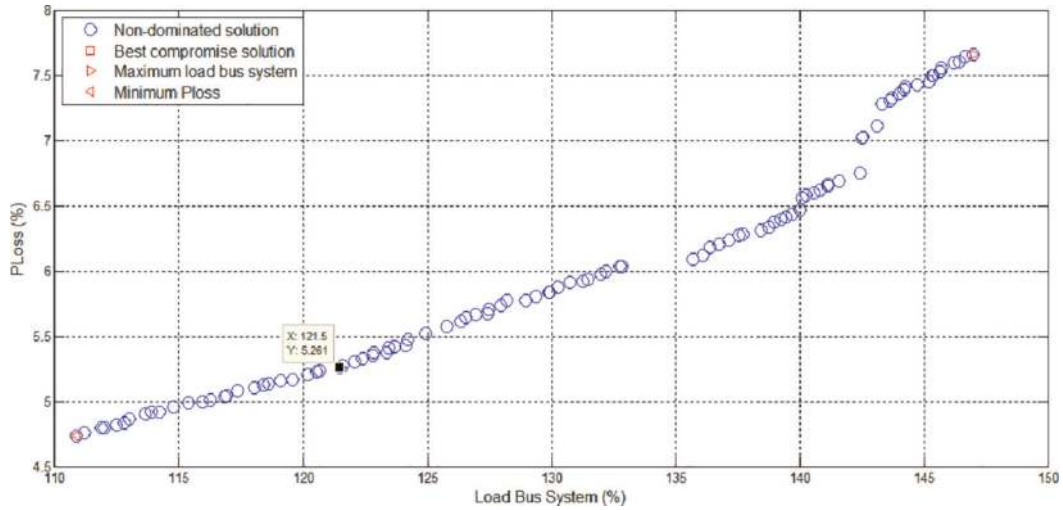**Figure 7.**
*The eigenvalue of Case-1.*

**Figure 8.**
*Pareto front of Case-2.*

it can be seen that for the best CS, optimal placement TCSC of 19.9599 p.u. on lines 15–12 results in an increase in LBS and $P_{loss}$ of 121.49% and 0.1655%, respectively. The $P_{loss}$ is better compared to the same solution in both previous cases; even though the LBS are slightly lower than in Case-1. While **Figure 9** depicts the eigenvalues for all conditions that meet the constraints of small-signal stability.

### 5.1.4 Case-3: WTG and TCSC

In case 3, with an optimal WTG placement of 54.55 MW and −16.06 MVar on bus-4 and a TCSC on lines 2–3 with an optimal setting of 20 p.u. is obtained the best CS for LBS and $P_{loss}$ of 130.9% and 6.805%, respectively, as illustrated in **Figure 10**. The LBS value achieved is the highest value of all cases for the IEEE 14-bus test system, although the Ploss is almost similar to the results in case 1. **Figures 11–13** present numerous system stability constraints, not only eigenvalues but also FVSI and LQP of less than one, which indicate the system is stable under different conditions for the best CS.
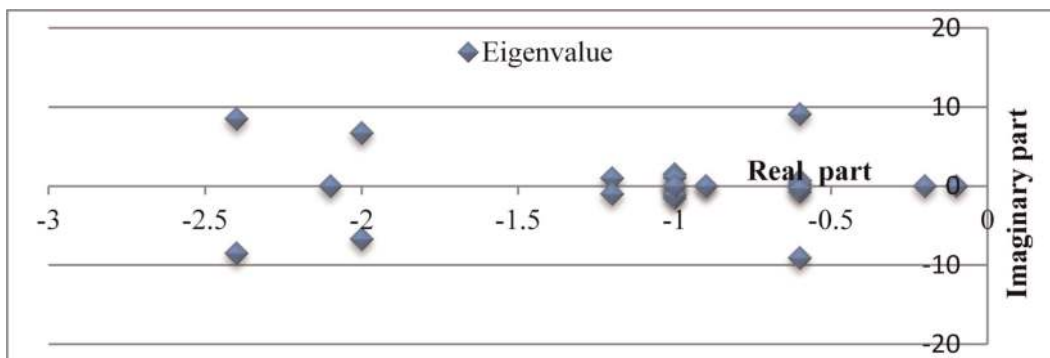


**Figure 9.**
*The eigenvalue of Case-2.*
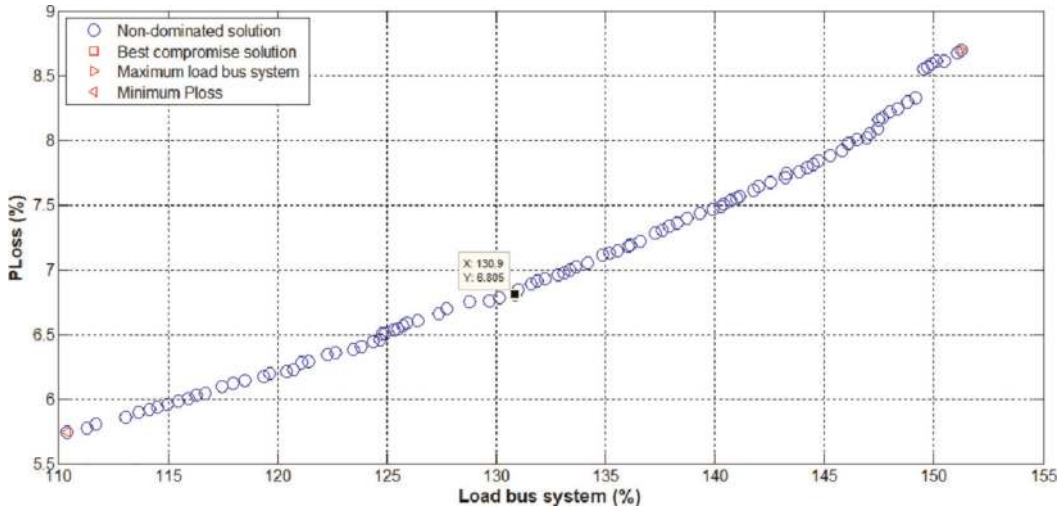
**Figure 10.**
*Pareto front of Case-3.*
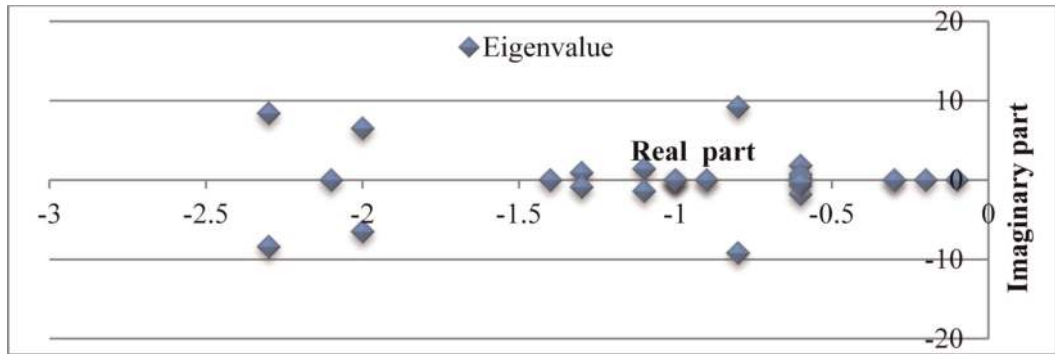


**Figure 11.**
*The eigenvalue of Case-3.*
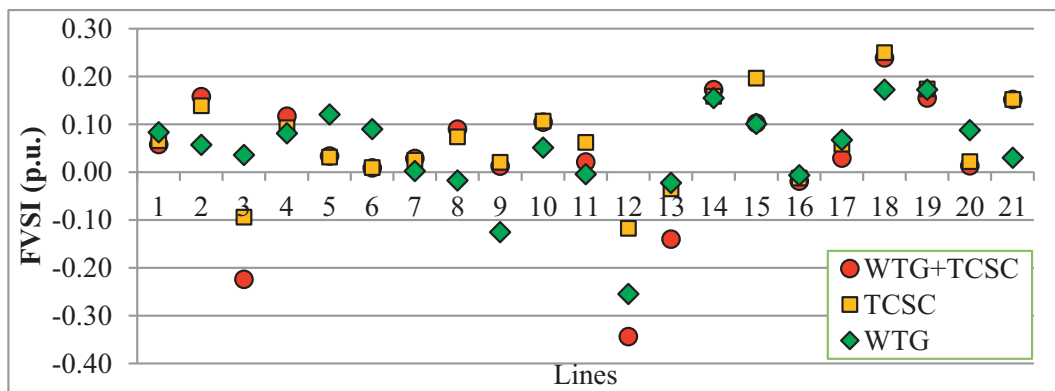


**Figure 12.**
*FVSI of Case-3.*

*5.1.5 Case-4: SVC only*

**Figure 14** presents the Pareto front of the best solution obtained in Case-4 by placing a shunt FACTS controller, SVC, on busses 9 and 5 with a setting of 1.01 p.u.
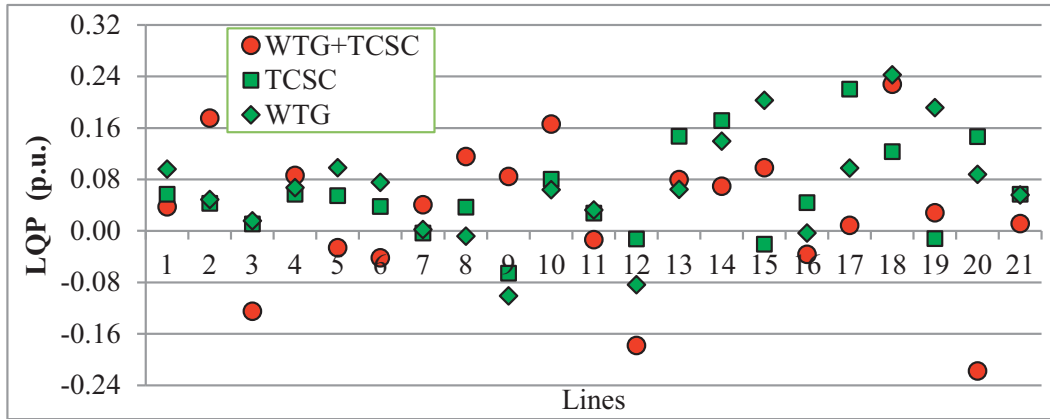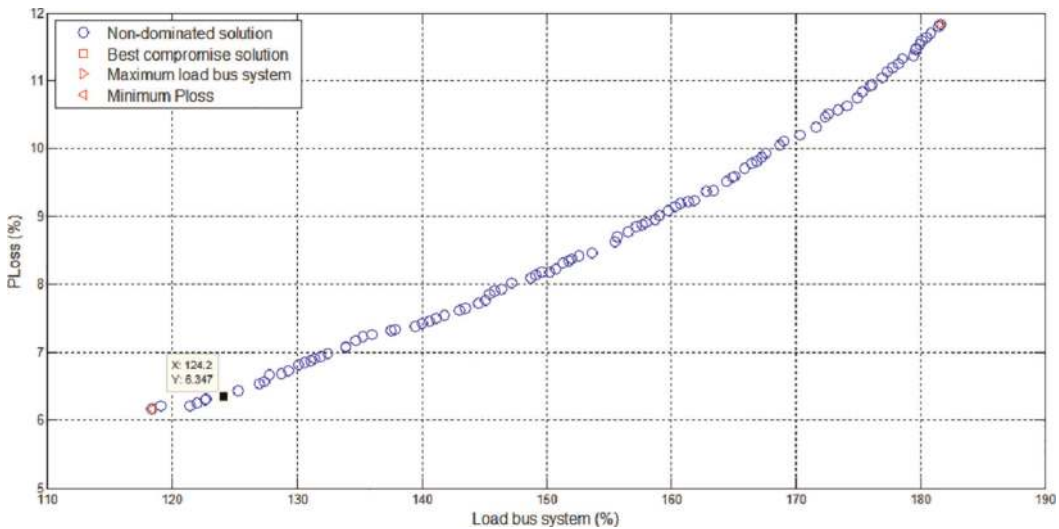
**Figure 13.**
*LQP of Case-3.*



**Figure 14.**
*Pareto front of Case-4.*

and 1.09 p.u., respectively. Max. LBS and Min. $P_{loss}$ reached 181.64% and 0.5562 p.u, respectively. Compared with the results of Case-1, the solution Min. $P_{loss}$ and Max. The LBS obtained in this case was slightly increased. **Figure 15** depicts a small signal stability constraint satisfied by placing SVC on bus-13, with a setting of 1.05 p.u. and giving the best CS LBS and $P_{loss}$ 124.16% and 0.2041 p.u, respectively.

### 5.1.6 Case-5: WTG and SVC

From the simulation results shown in **Figure 16** for Case-5, the best CS of LBS is 126.25% and $P_{loss}$ 0.2429 p.u with the optimal placement of SVC on bus-7 by settings of 0.6144 pu and WTG on bus-3 with active power and reactive power of 39.15 MW and −23.20 MVAr, respectively. In addition, from the Figure, Max. LBS and Min. $P_{loss}$ was 182.79% and 0.2107 pu, respectively, after placement of the shunt FACTS and WTG at their optimal locations. Compared to Cases 1 and 2, the best CS, in this case, is the highest. In all conditions, the eigenvalues of the stable system, as depicted in **Figure 17**.
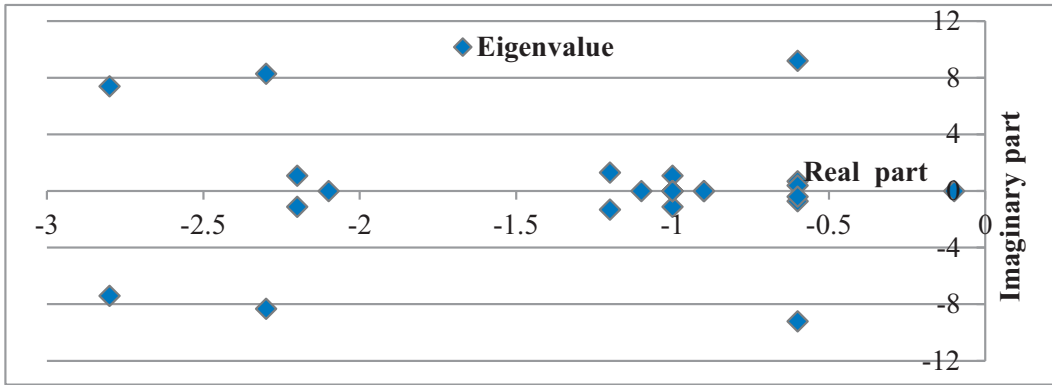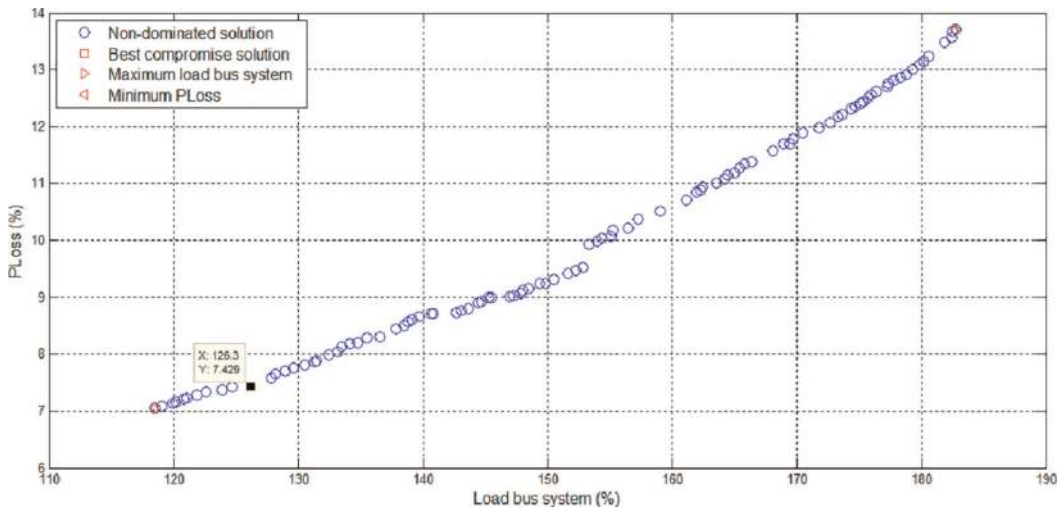
**Figure 15.**
*Eigenvalue of Case-4.*
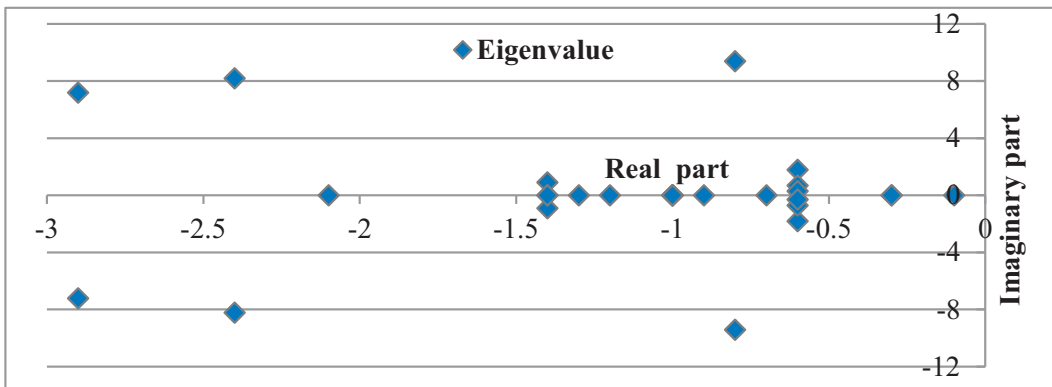


**Figure 16.**
*Pareto front of Case-5.*



**Figure 17.**
*Eigenvalue of Case-5.*

In order to maintain the stability of the network voltage at numerous LBS levels and guarantee that no line is overloaded, then the two system security indices have been considered in this Case-5 as depicted in **Figures 18** and **19**. Both figures prove
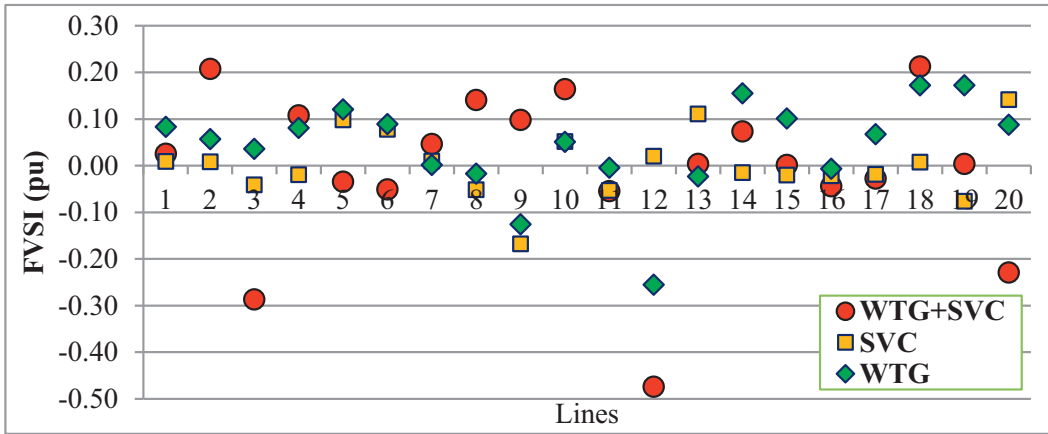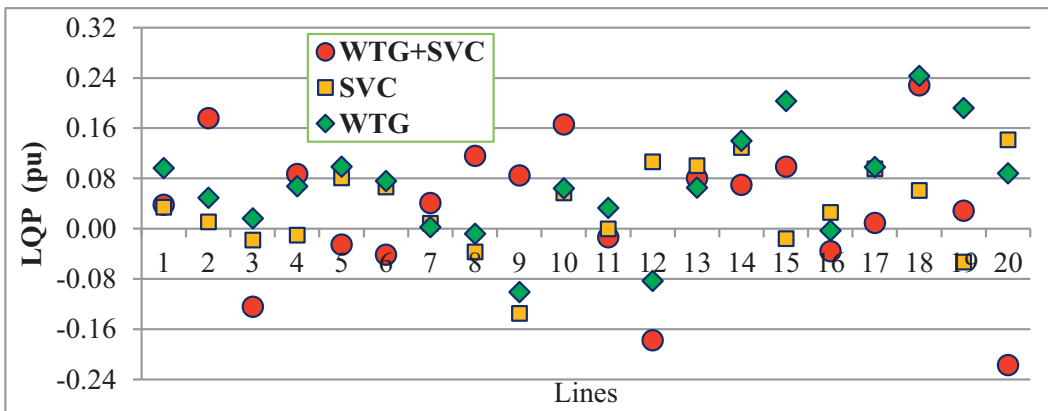
**Figure 18.**
*FVSI of Case-5.*



**Figure 19.**
*LQP of Case-5.*

that the FVSI and LPQ values for all cases, in this case, are less than 1.00, hence there is no bus collapse due to overload under any network conditions.

## 5.2 Practical test Indonesia Java-Bali 24-bus system

The developed method has also been successfully examined for its ability to modify the practical test system for 24 Java-Bali busses in Indonesia. Testing has been carried out to demonstrate more tangible results for all of the above case studies, but in this discussion, only the results are presented for Cases 3 and 5.

### 5.2.1 Case-3 for Java-Bali 24-bus system

The Pareto front result for Case-3 is depicted in **Figure 20**. This figure provides the integration of a WTG in the best locations on bus 12 with a size of 19.47 MW and −44.17 MVar and the optimal placing of a TCSC on lines 19–24 (GNDUL-NEWBLRJA) with the setting of −31.6923 p.u achieve the best CS results of
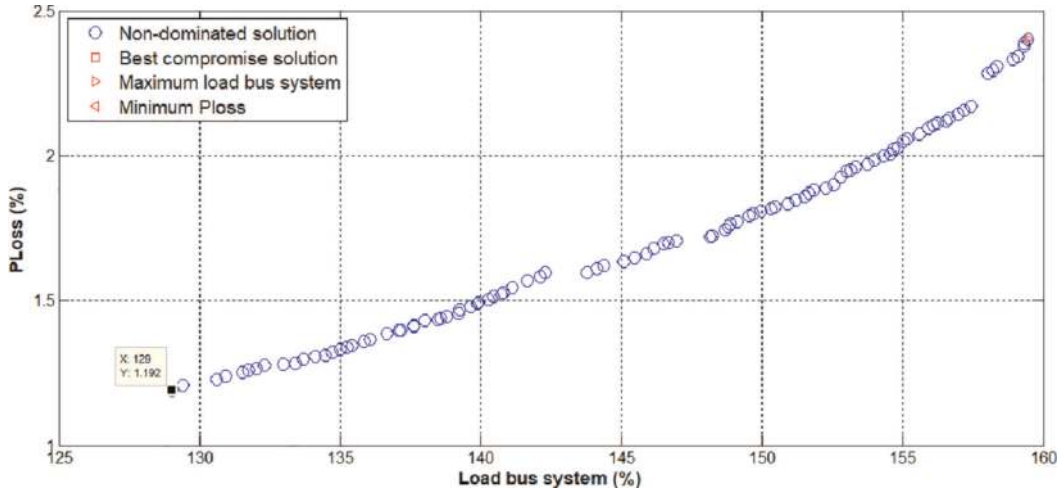
**Figure 20.**
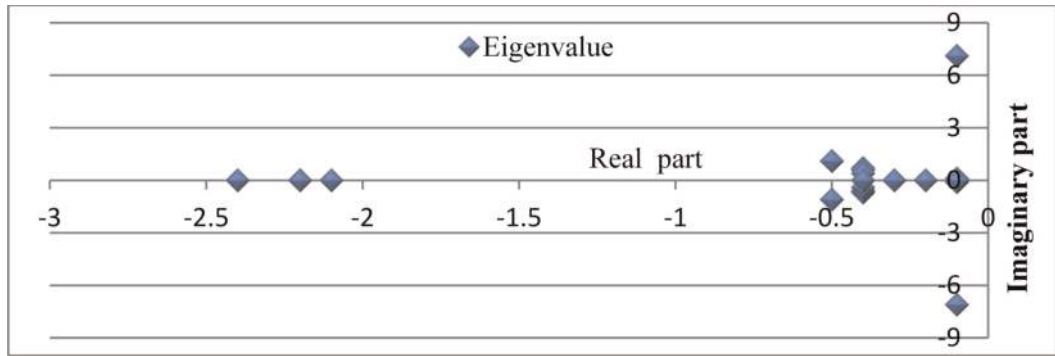*Pareto front of Case-3 for Indonesia Java-Bali 24-bus system.*



**Figure 21.**
*The eigenvalue of Case-3 for Indonesia Java-Bali 24-bus system.*
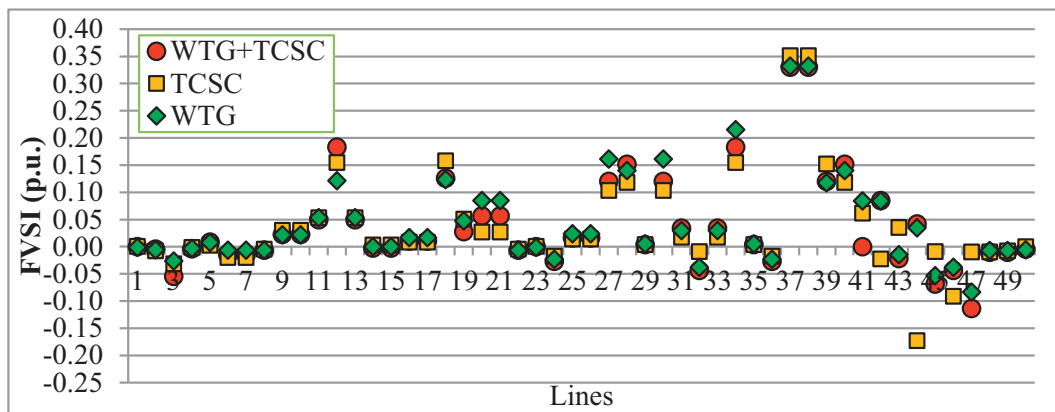


**Figure 22.**
*FVSI of Case-3 for Indonesia Java-Bali 24-bus system.*

optimal LBS and $P_{loss}$ of 129% and 1.1917%, respectively. All the system stability constraints, in this case, small-signal stability, FVSI, and LQP, are satisfied, as described in **Figures 21–23**.
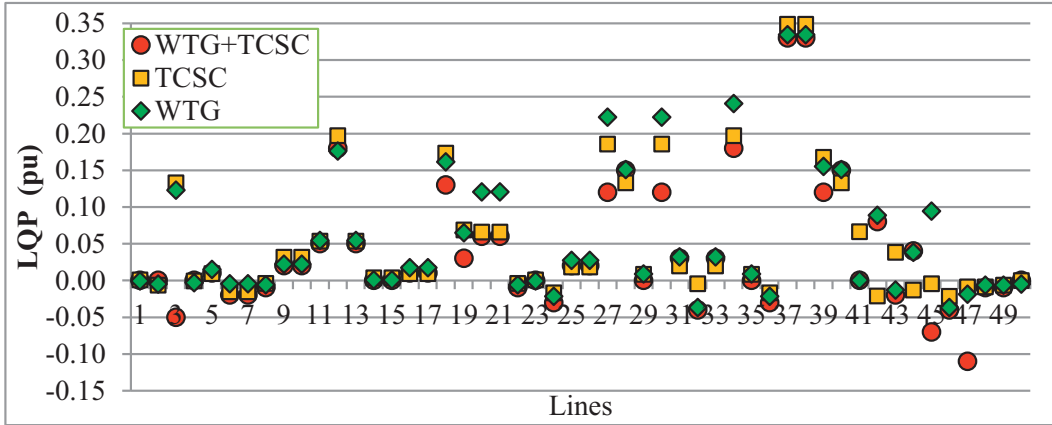
**Figure 23.**
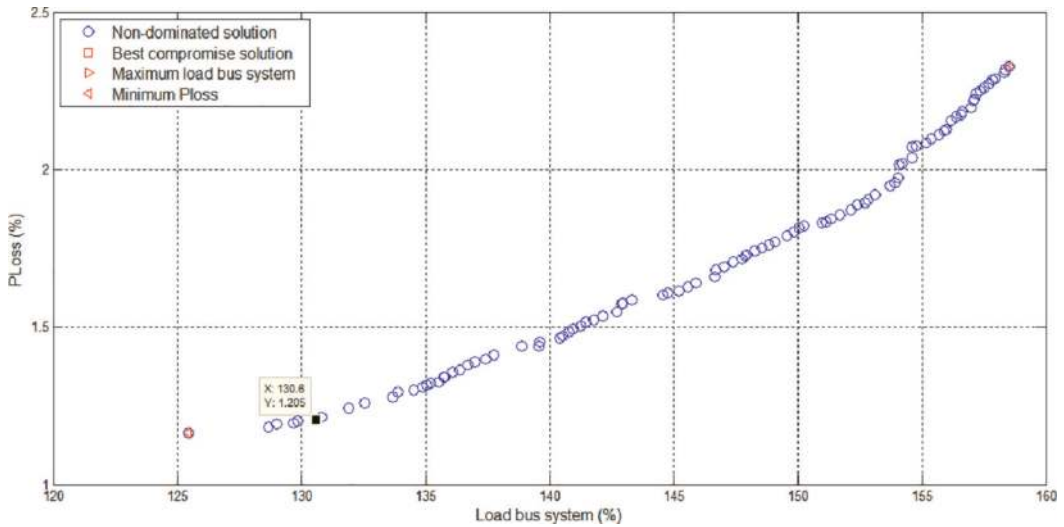*LQP of Case-3 for Indonesia Java-Bali 24-bus system.*



**Figure 24.**
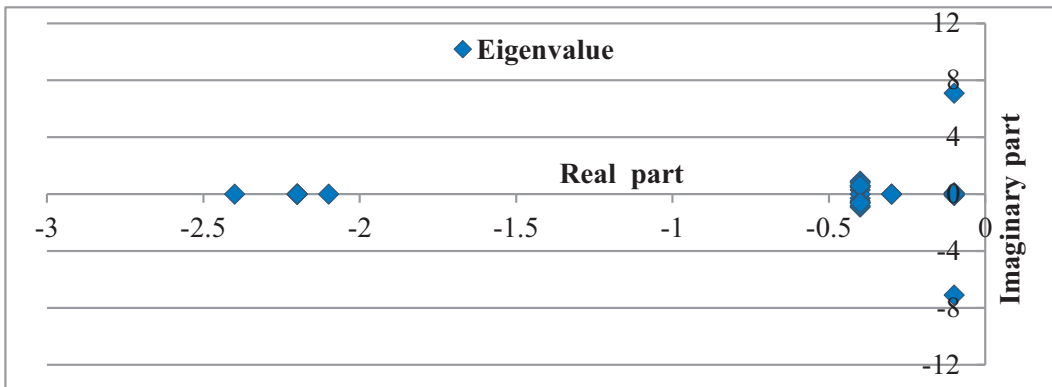*Pareto front of Case-5 for Indonesia Java-Bali 24-bus system.*



**Figure 25.**
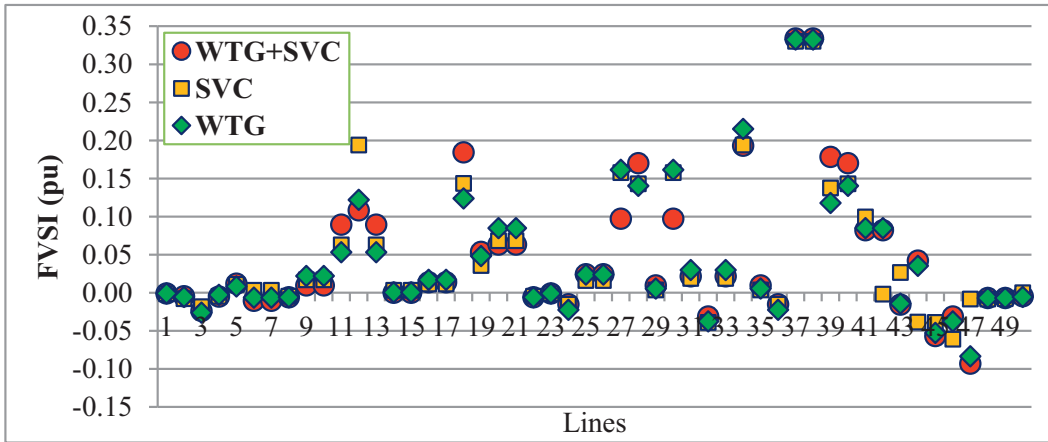*The eigenvalue of Case-5 for Indonesia Java-Bali 24-bus system.*

**Figure 26.**
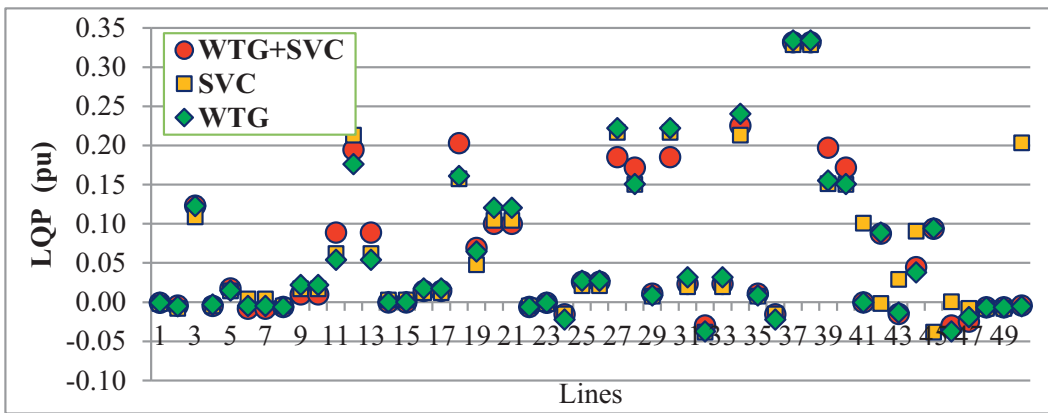*FVSI of Case-3 for Indonesia Java-Bali 24-bus system.*



**Figure 27.**
*LQP of Case-3 for Indonesia Java-Bali 24-bus system.*

*5.2.2 Case-5 for Java-Bali 24-bus system*

The results of the Pareto front simulation for Case-5 on the Indonesian Java-Bali 24-bus system with the integration of a WTG and placement of an SVC are shown in **Figure 24**. From the figure, it can be observed that installing a WTG on bus-19 and an SVC on bus-13 and gives Max. SLB and Min. Ploss of 158.54% and 3.90 p.u, respectively. While the best CS LBS is 130.63% by placing an SVC in the same position but a WTG on bus-16. System stability and security based on system eigenvalues, FVSI, and LQP which prove the system is stable on the best CS, are presented in **Figures 25–27**.

## 6. Conclusions

Many system stability and security index constraints viz.: small-signal stability, FVSI, and LQP and status of system security constraints, that is, line thermal limit and bus voltage violation limits, have been successfully investigated. The indexes are satisfied with all the limitations in the DFIG type WTG integrated grid system by

controlling two types of FACTS, TCSC and SVC. The problem formulated as a bi-optimization, maximizing the LBS system (Max. LBS), and minimizing $P_{loss}$ (Min. $P_{loss}$) is both conflicting. To make it an optimal solution, the placing, and sizing of WTG and the setting of the series and shunt FACTS controllers are carried out using NSGA-II multi-objective optimization techniques. With the NSGA-II optimization techniques, the problem of bi-objective formulation has been solved to determine various cases of a combination of optimal locations, WTG (wind farm) size, and TCSC and SVC controller settings in the grid. The multi-objective approach has been successfully tested for effectiveness in the IEEE 14-bus standard test system and the Indonesia Java Bali 24-bus practical test system. In all cases, the proposed technique can keep all system stability constraints and safety margins within safe limits. Furthermore, a fuzzy-based mechanism quotes the best CS from the Pareto front.

## Author details

I. Made Wartana* and Ni Putu Agustini
Department of Electrical Engineering, National Institute of Technology, Malang, Indonesia

*Address all correspondence to: m.wartana@lecturer.itn.ac.id

InLechOpen

## References

[1] Jeguirim M. Recent Advances in Renewable Energy Technologies. Elsevier; 2021

[2] Patel MR, Beik O. Wind and Solar Power Systems: Design, Analysis, and Operation. Boca Raton: CRC Press; 2021

[3] Ahmad J et al. Techno economic analysis of a wind-photovoltaic-biomass hybrid renewable energy system for rural electrification: A case study of Kallar Kahar. Energy. 2018;**148**: 208-234

[4] Răboacă MS et al. Concentrating solar power technologies. Energies. 2019; **12**(6):1048

[5] Nazir MS et al. Wind generation forecasting methods and proliferation of artificial neural network: A review of five years research trend. Sustainability. 2020;**12**(9):3778

[6] Paliwal P, Patidar N, Nema R. Planning of grid integrated distributed generators: A review of technology, objectives and techniques. Renewable and Sustainable Energy Reviews. 2014; **40**:557-570

[7] Shuaibu Hassan A, Sun Y, Wang Z. Optimization techniques applied for optimal planning and integration of renewable energy sources based on distributed generation: Recent trends. Cogentive Engineering. 2020;**7**(1): 1766394

[8] Rangu SK, Lolla PR, Dhenuvakonda KR, Singh AR. Recent trends in power management strategies for optimal operation of distributed energy resources in microgrids: A comprehensive review. International Journal of Energy Research. 2020; **44**(13):9889-9911

[9] Kim YJ, Kirtley JL, Norford LK. Reactive power ancillary service of synchronous DGs in coordination with voltage control devices. IEEE Transactions on Smart Grid. 2015;**8**(2): 515-527

[10] Selim A, Kamel S, Alghamdi AS, Jurado F. Optimal placement of DGs in distribution system using an improved Harris hawks optimizer based on single- and multi-objective approaches. IEEE Access. 2020;**8**:52815-52829

[11] Kumar NP, Rosalina KM. IPSO algorithm for maximization of system loadability, voltage stability and loss minimisation by optimal DG placement. System. 2015;**3**(11):73-77

[12] Kotsampopoulos P, Georgilakis P, Lagos DT, Kleftakis V, Hatziargyriou N. FACTS providing grid services: Applications and testing. Energies. 2019; **12**(13):2554:1-23

[13] Relić F, Marić P, Glavaš H, Petrović I. Influence of FACTS device implementation on performance of distribution network with integrated renewable energy sources. Energies. 2020;**13**(20):5516

[14] Gellings CW. The Smart Grid: Enabling Energy Efficiency and Demand Response. New York: River Publishers; 2020

[15] Liang X. Emerging power quality challenges due to integration of renewable energy sources. IEEE Transactions on Industry Applications. 2016;**53**(2):855-866

[16] Abdmouleh Z, Gastli A, Ben-Brahim L, Haouari M, Al-Emadi NA. Review of optimization techniques applied for the integration of distributed

generation from renewable energy sources. Renewable Energy. 2017;**113**: 266-280

[17] Shereen MA. Optimal allocation of DG units for radial distribution systems using genetic algorithm. International Journal of Engineering and Advanced Technology (IJEAT). 2012;**1**(6):175-179

[18] Farh HM, Al-Shaalan AM, Eltamaly AM, Al-Shamma AA. A novel crow search algorithm auto-drive PSO for optimal allocation and sizing of renewable distributed generation. IEEE Access. 2020;**8**:27807-27820

[19] Abdel-mawgoud H, Kamel S, Ebeed M, Aly MM. An efficient hybrid approach for optimal allocation of DG in radial distribution networks. In: 2018 International Conference on Innovative Trends in Computer Engineering (ITCE). IEEE; 2018. pp. 311-316

[20] Zad BB, Hasanvand H, Lobry J, Vallée F. Optimal reactive power control of DGs for voltage regulation of MV distribution systems using sensitivity analysis method and PSO algorithm. International Journal of Electrical Power & Energy Systems. 2015;**68**:52-60

[21] Kamarudin B, Hashim TJT, Musa A. Optimal Sizing and Location of Distributed Generation for Loss Minimization Using Firefly Algorithm. Indonesian Journal of Electrical Engineering and Computer Science. 2019;**14**(1):421-427

[22] Wartana I, Agustini NP, Singh JG. Optimal integration of the renewable energy to the grid by considering small signal stability constraint. International Journal of Electrical and Computer Engineering (IJECE). 2017;**7**(5)

[23] Nadjemi O, Nacer T, Hamidat A, Salhi H. Optimal hybrid PV/wind energy system sizing: Application of cuckoo search algorithm for Algerian dairy farms. Renewable and Sustainable Energy Reviews. 2017;**70**: 1352-1365

[24] Jamal T, Urmee T, Shafiullah G. Planning of off-grid power supply systems in remote areas using multi-criteria decision analysis. Energy. 2020; **201**:117580

[25] Islam MM, Muttaqi KM, Sutanto D. A novel saturated amorphous alloy core based fault current limiter for improving the low voltage ride through capability of doubly-fed induction generator based wind turbines. IEEE Transactions on Industry Applications. 2021;**57**(3): 2023-2034

[26] Mehta B, Bhatt P, Pandya V. Small signal stability analysis of power systems with DFIG based wind power penetration. International Journal of Electrical Power & Energy Systems. 2014;**58**:64-74

[27] Zhang C, Ke D, Sun Y, Chung C, Xu J, Shen F. Coordinated supplementary damping control of DFIG and PSS to suppress inter-area oscillations with optimally controlled plant dynamics. IEEE Transactions on Sustainable Energy. 2017;**9**(2):780-791

[28] Mohanty A, Viswavandya M, Mohanty S, Paramita P. Intelligent TCSC for enhancement of voltage stability and power oscillation damping of an off grid. In: Computational Intelligence in Data Mining. New Delhi: Springer; 2016. pp. 229-237

[29] Ziaee O, Choobineh FF. Optimal location-allocation of TCSC devices on a transmission network. IEEE Transactions on Power Systems. 2016; **32**(1):94-102

[30] Pati S, Dahiya R. Impact of wind integration on placement of TCSC. In: 2016 International Conference on Emerging Trends in Electrical Electronics & Sustainable Energy Systems (ICETEESES). IEEE; 2016. pp. 56-59

[31] Barrios-Martínez E, Ángeles-Camacho C. Technical comparison of FACTS controllers in parallel connection. Journal of Applied Research and Technology. 2017;**15**(1):36-44

[32] Agustini NP, Wartana IM, Lomi A. Improvement of static voltage stability of 16-bus bali system by optimal placement of SVC. International Journal of Smart Grid and Sustainable Energy Technologies. 2021;**4**(1):140-144

[33] Wartana IM, Singh JG, Ongsakul W, Sreedharan S. Optimal placement of FACTS controllers for maximising system loadability by PSO. International Journal of Power and Energy Conversion. 2013;**4**(1):9-33

[34] Wartana IM, Agustini NP. Application of Voltage and Lines Stability Index for Optimal Placement of Wind Energy with a System Load Increase Scenario

[35] Wartana IM, Singh JG, Ongsakul W, Buayai K, Sreedharan S. Optimal placement of UPFC for maximizing system loadability and minimize active power losses by NSGA-II. In: 2011 International Conference & Utility Exhibition on Power and Energy Systems: Issues and Prospects for Asia (ICUE). IEEE; 2011. pp. 1-8

[36] Milano F. An open source power system analysis toolbox. IEEE Transactions on Power Apparatus and Systems. 2005;**20**(3):1199-1206

[37] Pai M, Sen Gupta D, Padiyar K, Senroy N. Small Signal Analysis of Integrated Power Systems. New Delhi: Narosa Publishing House Pvt. Ltd.; 2016

[38] Agustini NP, Hayusman LM, Hidayat T, Wartana IM. Security and Stability Improvement of Power System Due to Interconnection of DG to the Grid. In: Proceedings of Second International Conference on Electrical Systems, Technology and Information 2015 (ICESTI 2015). Singapore: Springer; 2016. pp. 227-237

[39] Wartana IM. A multi-objective problems for optimal integration of the DG to the Grid using the NSGA-II. In: 2015 International Conference on Quality in Research (QiR). IEEE; 2015. pp. 106-110

[40] Deb K. A fast elitist non-dominated sorting genetic algorithm for multi-objective optimization: NSGA-2. IEEE Transactions on Evolutionary Computation. 2002;**6**(2):182-197

[41] Nicholas PE, Padmanaban K, Babu ML. Multi-objective optimization of laminated composite plate with diffused layer angles using non-dominated sorting genetic algorithm (NSGA-II). Advanced Composites Letters. 2014;**23**(4):403

[42] Agrawal S, Panigrahi BK, Tiwari MK. Multiobjective particle swarm algorithm with fuzzy clustering for electrical power dispatch. IEEE Transactions on Evolutionary Computation. 2008;**12**(5):529-541

[43] Zitzler E, Giannakoglou K, Tsahalis D, Periaux J, Papailiou K, Fogarty T. SPEA2: Improving the Strength Pareto Evolutionary Algorithm for Multiobjective Optimization. Vol. 952100. Barcelona: Proc of the EUROGEN Conf. Barcelona; 2002